A Highly Stretchable Capacitive-Based Strain Sensor Based on Metal Deposition and Laser Rastering

*Ozgur Atalay, Asli Atalay, Joshua Gafford, Hongqiang Wang, Robert Wood, and Conor Walsh**

Wearable sensing technology is an emerging area and can be utilized for human motion monitoring, physiology monitoring, and human–machine interaction. In this paper, a new manufacturing approach is presented to create highly stretchable and soft capacitance-based strain sensors. This involves a rapid surface modification technique based on direct-write laser rastering to create microstructured surfaces on prestrained elastomeric sheets. Then, to impart conductivity, sputtering technology is utilized to deposit aluminum and silver metal layers on the bottom and top surfaces of the elastomer sheet, creating a soft capacitor. During benchtop characterization of the sensors, this study demonstrates that the fabricated electrodes maintain their electrical conductivity up to the 250% strain, and the sensor shows a linear and repeatable output up to 85% strain. Finally, their potential is demonstrated for monitoring human motion and respiration through their integration into a wearable arm sleeve and a thoracic belt, respectively.

There is growing interest in the development of soft or miniature sensors for use in human motion monitoring,[1–6] human and machine interaction,[7–10] or physiology monitoring.[11–14] There are several manufacturing technologies and materials available for the creation of soft strain sensing structures. Silicone-based elastomers are suitable base materials due to their ability to be cast or spun in thin sheets and their high strain capabilities.[15–17] Strain sensors can be created by depositing conductive materials onto silicone substrates. For this purpose, metals are often employed as the conductive material. However, because metals are typically not stretchable beyond 1%–2% strain level, most studies focus on the geometric modification of underlying elastomers to cause the deposited metals to behave elastically under high strain.[18–25] Since the measurement of high levels of strain (e.g., 50% or greater) for detection of posture or movement of the human body, is required for wearable applications,[26] the maximum strain limit of soft sensors can be enhanced through the creation of buckling (or wrinkling)[22,27–29] structures on the elastomer surface which enable a greater level of strain while maintaining good conductivity. A number of approaches have been demonstrated in the literature to create buckled thin metal films on elastomer surfaces; the most widely used method involves prestraining the elastomeric structure.[30,31] Previous studies have shown that, while prestrain alone offers performance improvements in terms of stretchability, it can also be combined with surface modification methods (such as photolithography or chemical techniques) in order to increase the maximum strain as well as to enhance adhesion between the elastomer and metal layers for the manufacturing of soft sensors.[32,33] It is worth noting that the combination of prestrain and micromachining of the surface is especially important in the manufacturing of capacitive strain sensors. Since it is crucial to maintain a crack-free electrode surface for reliable capacitive sensor performance under applied strain, the combination of these two methods helps to increase the crack-free strain range of the conductive electrodes. However, lithographic techniques require precise control of the resist thickness and other processing parameters including intensity of light exposure and timing of exposure, etching, and development.[34] In addition, all fabrication work must take place in a clean environment. An alternative to photolithography is to use a molding process to produce the microstructured pattern (wavy structure) on the elastomer surface. However, the minimum achievable pattern spacing is limited by the process used to create the mold (≈100–200 μm for subtractive machining or additive printing) which significantly limits the electromechanical performance of the sensing device.[22]

In this work, we address challenges encountered in the previously mentioned approaches by proposing an easy and efficient new process for fabricating buckled surfaces with thin metal film on elastomeric substrates at the micrometer scale for the development of capacitance-based soft strain sensors. The micropatterned surface is defined by a combination of direct-write laser rastering and biaxial stretching. One of the primary contributions of our approach is that surface modification via laser treatment requires a single processing step compared to other approaches (such as lithographic or chemical techniques) which require multiple steps to create the desired pattern. In

Dr. O. Atalay, Dr. A. Atalay, J. Gafford, Dr. H. Wang, Prof. R. Wood, Prof. C. Walsh
Harvard John A. Paulson School of Engineering and Applied Sciences
Harvard University
Cambridge, MA 02138, USA
E-mail: walsh@seas.harvard.edu
Dr. O. Atalay, Dr. A. Atalay, J. Gafford, Dr. H. Wang, Prof. R. Wood, Prof. C. Walsh
Wyss Institute for Biologically Inspired Engineering
Harvard University
Boston, MA 02115, USA

DOI: 10.1002/admt.201700081

order to impart conductivity, sputtering technology was utilized to deposit metal layers on the bottom and top surfaces of the elastomer, and these conductive layers act as conductive plates in the proposed capacitive sensor design. In this paper, we investigate the strain-sensing characteristics of conductive electrodes as well as the soft capacitive sensors. We also demonstrated that the proposed sensor is a viable means of sensing gross and subtle human motion such as elbow flexing and respiratory motion. To assess potential efficacy as a wearable goniometry device, we integrated the sensor into a wearable sleeve and correlated arm bending angles and corresponding electrical output for elbow motion monitoring and characterization, with potential applications in wearable robotics and physical therapy. In addition, the sensor was integrated into a thoracic belt for measuring inhalation and exhalation of the respiration cycle.

The manufacturing process of the elastomeric conductive electrodes for soft capacitive sensors, as well as general electrodes for soft sensor design and implementation, is shown in **Figure 1**. The process can be divided into five steps; manufacturing the silicone elastomer substrate, surface microstructuring of the elastomer surface via laser treatment, prestraining of the elastomer (up to ≈80%), metal deposition on the elastomer surfaces, and releasing the prestrain and cutting into sensor strips. First, sequential line patterns are machined into the elastomer using a diode-pumped solid-state (DPSS) laser to create a pattern with thousands of linear microgrooves on the elastomer surface (Figure 1a; Video S1, Supporting Information). It should be noted here that laser machining parameters have substantial effects on the quality of surface treatment, and as such, were carefully selected power, scan speed, and number of passes through trial-and-error. To limit the parameter space, we fixed the laser speed at 200 mm s^{-1} for a single pass and power as 0.42 W (Figure S1, Supporting Information). Figure 1a shows optical microscopy images of the laser treated samples in which the micromachined channels are easily observed and are similar in nature to those patterned by photolithography or mold techniques demonstrated in previous works.[22,35,36] In our case, the laser rastering process creates a first-order pattern characterized by the microgrooves, as well as smaller-sized topographical features on the sidewalls of the microgrooves as a consequence of the ablation process (which help to increase overall surface roughness of the elastomer independent from the laser treatment direction) as shown in Figure 1a. For the untreated samples, the measured average surface roughness is 0.15 µm. The surface roughness of the laser treated samples is found to be 1.26 µm (Figure S2, Supporting Information) which serves to promote adhesion between the metal and the elastomer surface owing to an increase in the overall surface area.[37] Further research can be conducted to determine the effect of different patterns on the surface roughness of the treated elastomer. Figure 1b illustrates the complete manufacturing process of the conductive electrodes and subsequent sensor design. Colored dyes were added to the surface of the transparent elastomer to ensure uniform UV absorption across the entire elastomer surface, thereby creating a more homogeneous microstructure. After the laser treatment, the

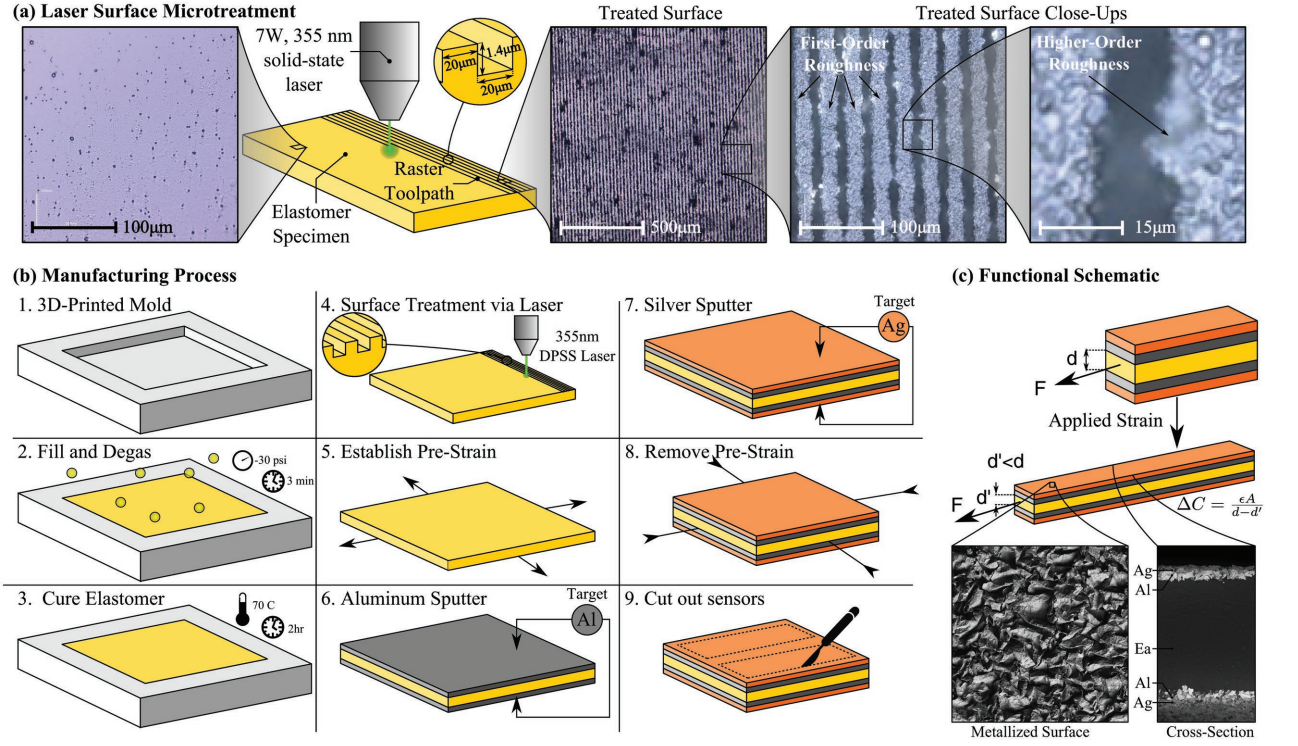

Figure 1. a) Schematic diagram of the laser raster process on the elastomer surface (insets show optical microscopy of the elastomer surface before and after laser raster). b) Schematic diagram of the fabrication process used to manufacture the conductive electrodes and capacitive soft sensors. c) 3D illustration of the sensor and general working principle (insets show a cross sectional view of the sensor and surface image of electrode area captured via SEM).

microstructured silicone elastomers were then prestrained biaxially prior to metal deposition. Aluminum was first sputtered onto the elastomer surface to promote adhesion between the elastomer and the silver layer that was subsequently deposited on top of the aluminum layer. The prestrain was then removed and discrete sensor strips were cut out from the continuum structure. Figure 1c; and Figure S3 (Supporting Information) show a functional schematic of the capacitive sensors as well as scanning electron microscope (SEM) images of the electrode layer. The metal layers on the top and bottom faces of the silicone elastomer act as conductive electrodes, and the silicone elastomer between them acts as the dielectric layer. Thus an inherent advantage of this manufacturing approach is that one layer of silicone elastomer is sufficient to accommodate both the electrode and dielectric part of the capacitive sensor. It is worth noting that the principal loading direction of the sensor is determined by a combination of direct laser rastering and prestrain. Since the silicone elastomers are prestrained bi-axially, the principal loading direction of the sensor is both parallel and perpendicular to the raster tool path. However, for testing purposes in this study, the loading direction was chosen to be perpendicular to the raster tool path in order to utilize the combined effect of laser treatment and prestrain.

The sensor can be treated as a simple parallel-plate capacitor with a dielectric layer that varies in thickness as the sensor is strained axially. Thus, as a result of the decrease in thickness due to an applied strain, the sensor's total capacitance increases. The capacitance of the sensor is given by

$$C_0 = \varepsilon_o \varepsilon_r l_0 w_0 / d_0' \tag{1}$$

where C_0 represents the capacitance value of the sensor, ε_o and ε_r are permittivities associated with free space and the dielectric layer respectively, l_0 and w_0 are length and width of the electrode area respectively, and d_0' is the distance separating the two electrodes. As the capacitive sensor is stretched, the length of the electrode increases to $(1 + \varepsilon)l_0$, while the width of the electrode decreases to $(1-\nu_{electrode})w_0$ and the separation between the two electrodes decreases to $(1-\nu_{dielectric})d_0'$ (where ε is the strain value, $\nu_{electrode}$ and $\nu_{dielectric}$ are the Poisson ratios of the electrode and dielectric layer, respectively). Since the electrode and dielectric layers of the sensor are made of the same silicone elastomer, the capacitance of the proposed sensor under tensile strain can be predicted as follows [38]

$$\begin{aligned} C &= \varepsilon_o \varepsilon_r \frac{(1+\varepsilon)\, l_0 (1-\nu_{electrode})\, w_0}{(1-\nu_{dielectric})\, d_0'} \\ &= \varepsilon_o \varepsilon_r \frac{(1+\varepsilon) l_0 w_0}{d_0'} \\ &= (1+\varepsilon) C_0 \end{aligned} \tag{2}$$

While controllable microcracks are desirable and successfully implemented for the production of resistive-based strain sensors,[39] for capacitive strain sensors, the constant conductivity, and stable overlapped area of the electrodes is a key factor in realizing reliable and repeatable sensor measurement.[38] Since the soft capacitive strain sensor was devised with a configuration similar to that of a parallel plate capacitor, the conductive properties of the electrodes affect the overall performance of the capacitive sensor, and it is crucial to determine the strain range over which crack propagation is minimal such that the change in capacitance is predominantly due to the change in electrode geometry. As long-range crack propagation introduces discontinuities within the metal-deposited area, the conductive pathway and overlapped conductive electrode area are effectively reduced, thereby adversely affecting sensor linearity and sensitivity.

For characterizing the electrical response of the conductive electrodes to mechanical strain, we developed an experimental setup to collect synchronized mechanical and electrical data, using a custom-designed mechanical testing platform and a MATLAB xPC real-time target system for position control and data acquisition.[40] The resistance was measured by configuring the conductive elastomer as one leg of a voltage divider in series with a 4 Ω power resistor, and measuring the voltage at the midpoint. Connections to the sensor were made using 2 mm by 1 mm conductive disc magnets which were placed onto the elastomer surface from both sides, and we soldered Micro coaxial cable (50MCX-37, Molex Temp-Flex, USA) onto the magnets as signal transmission lines to connect to data acquisition electronics.

Initially, to investigate the standalone effect of laser treatment on the conductivity of the metallized electrodes, the normalized change-in-resistance (R/R_0, where R_0 is defined as the initial resistance of the as-prepared sample) was measured under increasing strain until conductivity was ultimately lost (i.e., the output voltage from the voltage divider drops to zero). As shown in **Figure 2**a, upon the application of increasing tensile strain, laser treated conductive electrodes remained conductive for strains as large as 66%, compared to values previously reported in the range of 20%–30%.[22,35–37] As shown in previous works,[41–44] topographical features (e.g., nanoscale pyramids, microstructured line patterns, micrometer-scale circular pillars) on elastomer surfaces provide sites for strain localization, thereby preventing large crack propagation. In our case, linear microgrooves on the elastomer surface also worked as sites for strain localization in conjunction with higher order pattern features on the sidewalls of the microgrooves that manifest as a consequence of the laser ablation process which serve to promote adhesion and create additional strain localization areas, thereby increasing the maximum strain limit of the sensor. Although the nonlaser treated samples were electrically conductive after metal deposition, the metal layers had a tendency to delaminate from the elastomer substrates under low strain, i.e., 1%<, and as such, simply handling the samples caused them to lose conductivity, thereby making it difficult to systematically characterize their electromechanical behavior.

The conductive properties of the electrodes can also be tuned by adjusting the distance between the microgrooves (hereafter referred to as the pitch). It should be noted here that 20 μm pitch was the minimum value we could achieve as this is approximately the spot-size of the laser and we also machined samples with pitches of 50 μm for comparison. As shown in Figure 2a, samples with 20 μm pitch maintained their electrical conductivity up to higher levels of strain when compared to the samples with 50 μm pitch. Since externally applied strain on a patterned sample manifests as a change in the surface

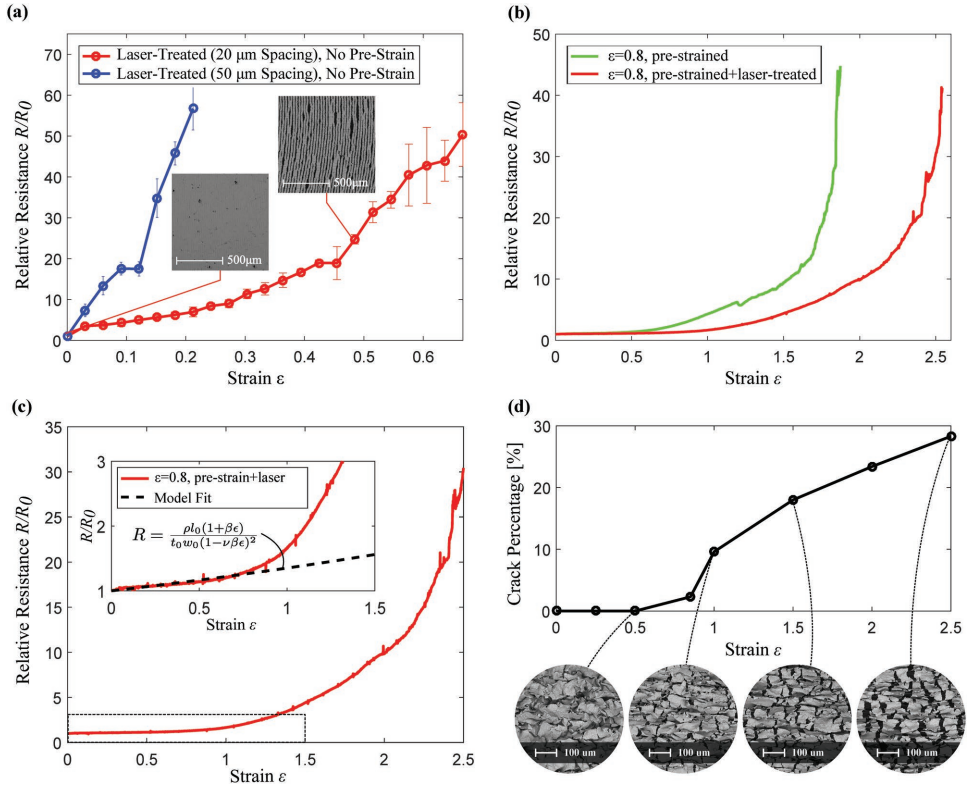

Figure 2. Performance characterization of conductive elastomers as stretchable conductors: a) Relative change in resistance for the laser treated samples with 20 and 50 μm pitch (no prestrain) up to the strain level at which conductivity is lost. b) Relative change in resistance for the samples with the prestrain of $\varepsilon = 0.8$ and laser treated sample with $\varepsilon = 0.8$ prestrain up to the strain level at which conductivity is lost. c) Relative change in resistance for the $\varepsilon = 0.8$ prestrained and laser-treated sample (inset shows theoretical electromechanical behavior of conductive electrode under applied strain), and d) change in crack area over the metal coated elastomer surface under the applied strain for prestrained and laser treated samples.

profile, when the pitch size decreases, the density of the microstructured pattern on elastomer surface increases which leads to greater strain relief on the elastomer surface, thereby enabling the electrodes to maintain their conductivity up to higher strains.

As demonstrated in Figure 2a, the creation of microstructures using laser treatment is an effective method to increase the maximum strain level of conductive electrodes. However, as described previously and illustrated in Figure 1, our combined approach for conductive electrode construction includes prestraining of microstructured samples before metal deposition, which was achieved using a rigid acrylic substrate and binder clips as described in the Experimental Section. We tested samples which were manufactured using the combined approach (prestrained, laser-treated) in order to observe the effect of strain on electrode conductivity. Samples were clamped into the mechanical testing setup and strained up to the level at which they lose their electrical conductivity. As seen in Figure 2b, samples manufactured using the combined approach maintained their electrical conductivity up to $\varepsilon = 2.5$. The plot also shows two distinct regions of strain response. In the first region from, $\varepsilon = 0$ to $\varepsilon = 0.85$, the change in resistance values only increased by a factor of 0.38 and the change in resistance is likely dominated by the change in buckling geometry and electrode geometry. This is illustrated by the inset of Figure 2c, which shows a close-up of the low-strain behavior compared to a model of resistance based purely on the change in sensor geometry as given by the following

$$R = \frac{\rho l_0 (1+\beta\varepsilon)}{w_0 t_0 (1-\nu\beta\varepsilon)^2} \tag{3}$$

where R is the instantaneous resistance, ρ is the resistivity of the silver layer, β is an empirical coefficient that accounts for the effects of prestrain, l_0 is the unstretched gage length of the sensor, w_0 is the sensor width, t_0 is the thickness of the silver layer, and ν is the Poisson ratio.

In the second region, from strains $\varepsilon = 0.85$ to $\varepsilon = 2.5$, the resistance of the samples increased rapidly due to the fracturing of the metal film on the elastomer surface which caused gaps within the metal film (see Figure 2d). As a result, the conductive pathway within the structure was reduced and the electrical resistance increased significantly. To validate this claim, we performed image analysis by using ImageJ to process SEM images of the sensor under different strain conditions (Figure S4, Supporting Information), allowing us to calculate the cracked area on the metal deposited sample as a percentage of the overall surface area of the sample. As seen Figure 2d, while the cracked area percentage was only 2.3% at the $\varepsilon = 0.85$ strain level, it reached 28.3% at the $\varepsilon = 2.5$ strain level. We also tested prestrained samples without laser treatment for comparison purposes. As seen Figure 2b, the change in resistance values

increased by a factor of 1.91 at the strain level of $\varepsilon = 0.85$ and samples maintained their conductivity up to a level of $\varepsilon = 1.87$ strain which indicates that our combined approach has increased the maximum strain values of the samples compared to nonlaser treated samples.

To demonstrate the conductivity of the deposited metals, the electrode was configured to pass current to a light-emitting diode (LED) under high strain. The LED remained lit as the electrode was stretched up to $\varepsilon = 2$ and finally the LED turned off at a strain level of $\varepsilon = 2.5$ (Figure S5, Supporting Information).

As shown in Figure 2c,d, crack area percentage within the metal layer is only 2.3% up to of $\varepsilon = 0.85$, and as such we chose this strain level for the recommended operating range of the soft capacitive sensor. We characterized the sensor's capacitive behavior using a commercial mechanical tester (Instron 5544A, Instron, USA) and a capacitance meter (Model 3000, GLK Instruments, USA). **Figure 3** presents the electromechanical results of the capacitive soft sensors that were manufactured using our combined approach. Figure 3a shows the capacitive response of the sensor during loading and unloading phases. With a maximum strain limit of $\varepsilon = 0.85$, the empirical data are well-fit by a linear regression model ($R^2 = 0.998$). The gauge factor ($\Delta C/C_0$) of the sensor is found to be 0.90, and hysteresis negligible at 24 mm s^{-1} cross head speed. To determine sensor resolution, we measured the noise in the sensor response at the maximum strain level of 85%. All measurements were obtained while maintaining a sensing bandwidth of 50 Hz. The resolution corresponds to a 95% confidence interval around the measured value. We found the absolute resolution value as 1.16% of full scale. Considering the gage length $l_0 = 40$ mm of the tested sensor, extensions well below a millimeter can be detected.

Sensor robustness over repeated cycles was tested for strain levels of $\varepsilon = 0.20$, 0.50, 0.80, and 1.00. The results are shown in Figure 3b. We observe that, for strain values up to the operating range of $\varepsilon = 0.80$, the relative capacitance decreases initially but stabilizes to a steady-state value, as the sensors remain in the strain regime where electrical characteristics are geometry-dominated, and the initial decrease is likely due to the viscoelastic properties of the elastomer layer. However, at $\varepsilon = 1.0$, the capacitance continues to decrease for subsequent cycles due to successive crack formation in the metallized layers which serves to reduce the overall plate area, thereby reducing capacitance.

The transient characteristics of the sensor's behavior are important to quantify, especially for dynamic applications. As shown in Figure 3c, $\varepsilon = 0.25$, 0.50, and 0.85 strain levels were applied to the capacitive sensor at a strain ramping rate of 3 mm s^{-1} and held for 20 s at these strain levels in order to observe the drift under static loading. Drift was calculated as the change in the sensor response to a constant strain value. The drift of the capacitance values of the strain sensor were measured to be 0.5%, 0.4%, and 0.2% for strain levels of $\varepsilon = 0.2$, 0.4, and 0.85, respectively. The response time of the

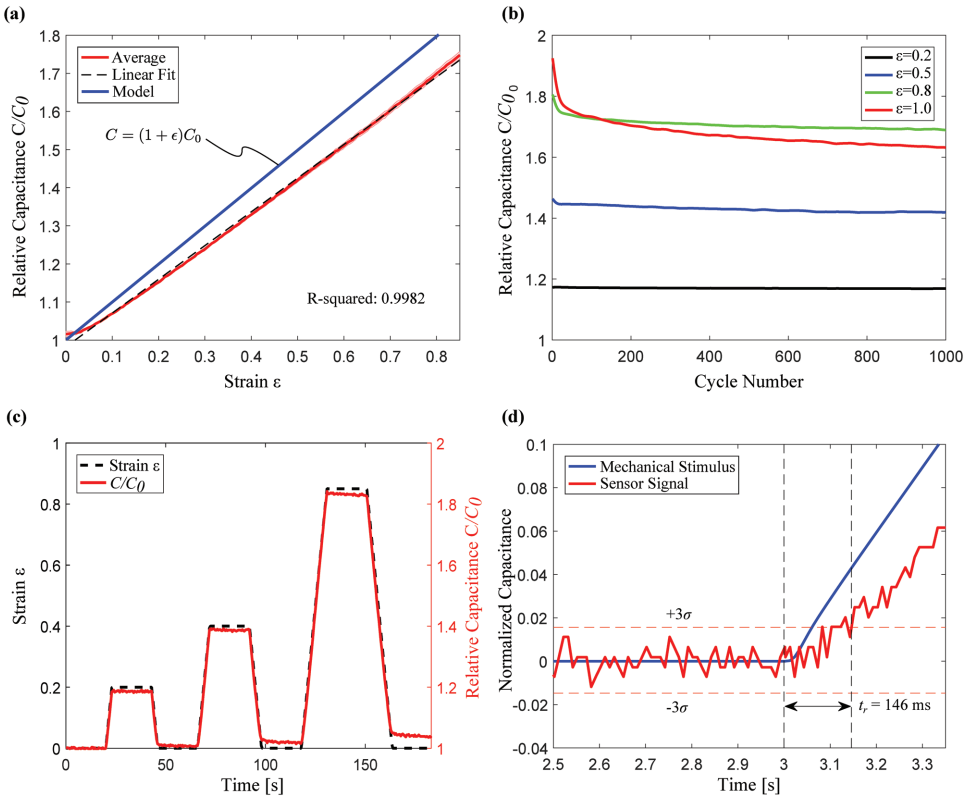

Figure 3. a) Capacitive response of a strain sensor up to strain level of $\varepsilon = 0.85$ as well as the linear fit (black line). b) Relative capacitance change as a function of cycle number for $\varepsilon = 0.2$, 0.4, 0.8, and 1 strain levels. c) Capacitance change as a function of time for sensors subjected to step deformation at $\varepsilon = 0.2$, 0.4, and 0.85 strain levels. d) Response time of the sensor.

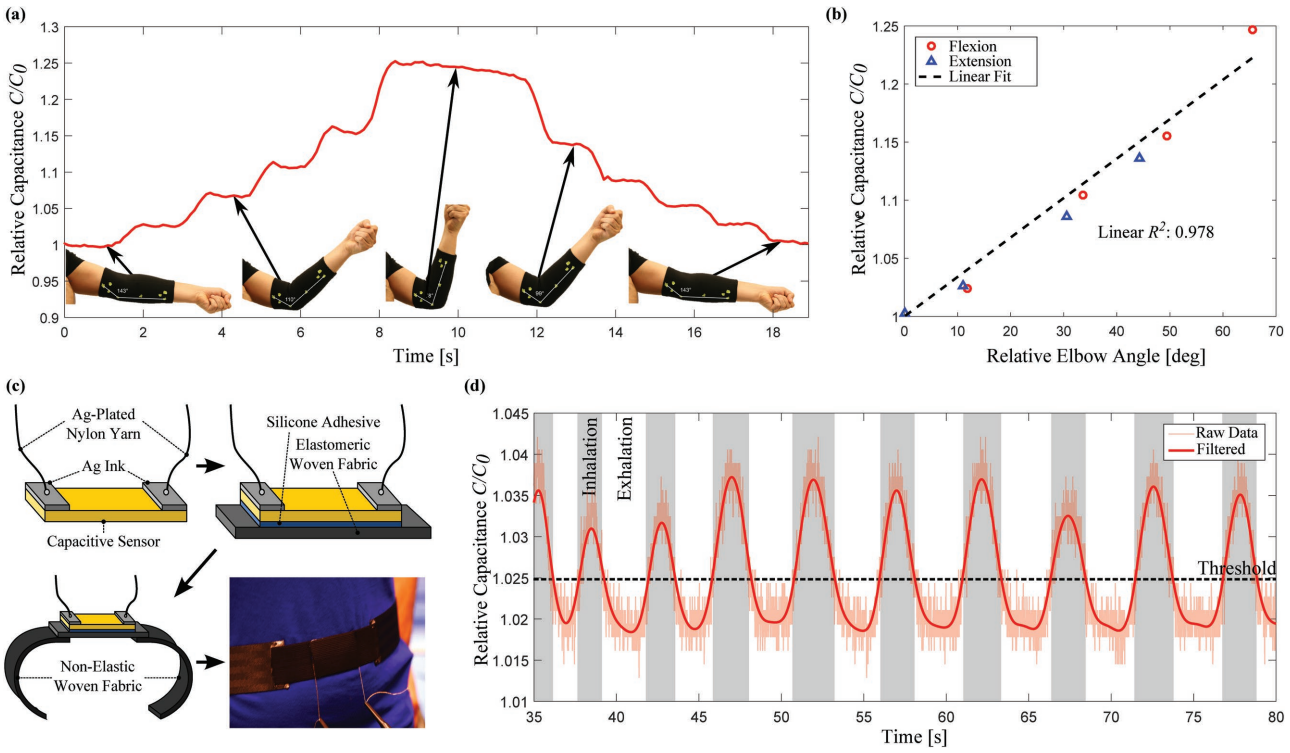

Figure 4. Capacitive soft sensor was used to monitor elbow movement and respiration. a) Change in capacitance while bending the strain sensor at the elbow joint. b) Relative capacitance value of the sensor versus bending angle. c) Manufacturing steps of the respiration belt. d) Sensor located on abdomen area for respiration rate monitoring.

sensor was calculated as the time span between mechanical stimulation and the point in time when the sensor signal rose three standard deviations above the base signal. The sensor's delay was found to be 0.146 ms (Figure 3d). Given that the frequency of body motion is usually below 10 Hz, our capacitive sensor could be considered a suitable candidate for sensing body motions.

In order to demonstrate the utility of the proposed sensor as a wearable device as shown in **Figure 4**, the strain sensor was used to monitor elbow movement during flexion and extension as well as respiration monitoring during inhalation and exhalation. For the monitoring of elbow movement, the capacitive sensor was mounted onto an elastic knit fabric arm sleeve using silicone rubber adhesive (Sil-Poxy, Smooth-on) and worn by the subject. Elbow angle measurements were taken during flexion and extension as shown in Figure 4a, and the capacitance of the sensor was simultaneously recorded. In order to measure flexion and extension angles, we placed markers on designated area of arm sleeve. Thereafter, we employed image analysis to measure relative angle changes during the activity. The relation between the bending angles and capacitance values of the sensor is shown in Figure 4b. The coefficient of determination (R^2) is 0.977 for a linear regression.

We also developed a respiration belt in order to monitor respiration activity as shown in Figure 4c. This could be useful in studies for monitoring the biomechanical and physiological response of wearers from assistance with soft wearable robots.[45] In order to manufacture the respiration belt, the capacitive sensor was mounted on elastomeric woven fabric using a silicone rubber adhesive (Sil-Poxy, Smooth-on). We applied silver ink at the edges of the sensor for the connection to the silver-plated nylon yarn (Shildex, USA) which provides signal transmission between the soft sensor and readout electronics. As a final step, we connected elastomeric woven fabric to non-elastomeric woven fabrics using fabric glue. The subject wore respiration belt while in a sitting position and was instructed to breathe normally. The peaks in the sensor output represent the inhalation, and the valley values represent exhalation, and simple thresholding can be used on the sensor data to clearly delineate the two. Through these examples, we have demonstrated that the sensors could be used for monitoring both vigorous human motion (elbow flexion and extension) as well as subtle motions (respiration). However, additional research is needed to further characterize the sensor in real life applications where direct contact with skin could introduce thermal gradients, potentially affecting the sensor's performance.

In this work, we report a new technique to fabricate highly stretchable microstructured metal electrodes for the manufacturing of capacitance-based soft strain sensors. This is achieved via the combination of direct-write laser rastering and biaxial prestrain that can create wrinkled elastomer surfaces to greatly improve the stretchability of soft sensors and conductive electrodes, and sputtering technology is used to deposit metal on elastomer surfaces. Conductive electrodes maintained their conductivity up to 250% strain and capacitive soft sensors produced a linear output up to 85% strain thanks to the electromechanical characteristics of the conductive electrode area. Finally, we demonstrate the application of the capacitance-based soft

strain sensors for detecting elbow movement and respiration monitoring. We envision that this type of soft strain sensors will also have suitability to be integrated into soft wearable robots for assisting with mobility and grasping[46–49] and some successful implementations have already been demonstrated in the recent literature.[50,51]

Experimental Section

Manufacturing of Silicone Elastomer: To fabricate the silicone elastomer, Dragon Skin 10 Slow cure (from Smooth-On) Part A and Part B were mixed in a ratio of 1:1 by weight with a centrifugal planetary mixer (ARE-310, Thinky Mixer USA) for 60 s. Blue silicone pigment (Silc PIG) was then added into the mixture (as 2% of total mixture weight) and whole mixture was further mixed for 60 s. Thereafter, the liquid silicone mixture (2.5 g) was subsequently poured into the 3D-printed mold. The mixture was degassed at −30 psi for 3 min before curing in the oven at 70 °C for 2 h.

Laser Treatment of Cured Elastomer: The cured elastomer was placed onto a glass slide and then placed into the Oxford Laser Systems DPSS laser micromachining system. The stage speed, number of passes, and laser power were chosen to be 200 mm m^{-1}, 1, and 0.42 W, respectively.

Prestraining of Laser Treated Samples: Samples were placed onto a rigid acrylic substrate and biaxially stretched manually using binder clips. Dimensions of the acrylic substrates were adjusted depending on the final dimension of the stretched elastomer.

Metal Deposition on Elastomer Surfaces and Sensor Construction: The thin film deposition process used in this work was physical vapor deposition. The sputtering chamber (Denton vacuum, LLC) was first evacuated to a base pressure of 2×10^{-4} torr prior to introducing the high purity argon gas as the bombardment gas. Voltage and current were selected as 600 mV and 500 mA, respectively. Initially, aluminum was coated onto the elastomer surface for 60 s. Silver was subsequently coated on top of the aluminum surface for 120 s. Thereafter, the same production settings were applied in order to deposit metal on the opposite surface of the elastomer for the completion of the parallel plate capacitor design. After metal deposition, the prestrain was released and the elastomer was cut into several sensor strips with the dimensions of 6 mm × 50 mm.

Calculation of the Surface Roughness of the Elastomer after Laser Treatment: Surface roughness of the samples were measured by LSM (Model: LE *Electrical Connections*: Electrical connections are established for signal acquisition and processing for the both electrodes and the complete sensor. For this purpose, 2 mm by 1 mm conductive disc magnets were used which placed onto the elastomer surface from both sides. Thereafter, Micro coaxial cable (50MCX-37, Molex Temp-Flex, USA) onto the magnets was soldered.

Electromechanical Tests for Conductive Electrodes: Conductive strips with dimensions of 6 mm by 50 mm were clamped into the tensile testing machine. The change in resistance was measured by configuring the electrode as a resistor in series with a 5 Ω power resistor in a voltage divider circuit and measuring the output voltage given a 5 V input. Analog voltage data were collected at a rate of 500 Hz. Due to the high sampling rate, the plots appear as if they are continuous despite representing discrete measurements in time.

Electromechanical Characterization of Capacitive Sensors: Sensors were dynamically tested in the tensile testing machine and capacitance was measured during testing with a capacitance meter (Model 3000, GLK instruments CA, USA). Load, extension, and capacitance data were synchronously logged via a common I/O interface, (bNC-2111, national Instruments Corp.), analog voltage data were collected at a rate of 100 HZ for capacitance measurements. Subject gave informed consent and testing was approved by the Harvard Medical School Institutional Review Board (IRB).

Supporting Information

Supporting Information is available from the Wiley Online Library or from the author.

Acknowledgements

This material is based upon the work supported by the National Science Foundation (Grant No. CBET-1454472), the Scientific and Technological Research Council of Turkey (TUBİTAK) BIDEB-2219Postdoctoral Research program and the Defense Advanced Research Projects Agency (DARPA), Warrior Web Program(Contract No. W911NF-14-C-0051), the Wyss Institute and the John A. Paulson School of Engineering and Applied Sciences at Harvard University. The authors also would like to thank James Weaver and Sven Engelhardt for SEM images.

Conflict of Interest

The authors declare no conflict of interest.

Keywords

capacitive sensors, laser rastering, soft strain sensors, sputtering, surface microtreatment

Received: March 29, 2017
Revised: May 10, 2017
Published online:

[1] Y. Mengüç, Y.-L. Park, H. Pei, D. Vogt, P. M. Aubin, E. Winchell, L. Fluke, L. Stirling, R. J. Wood, C. J. Walsh, *Int. J. Rob. Res.* **2014**, *33*, 1748.
[2] A. Frutiger, J. T. Muth, D. M. Vogt, Y. Mengüç, A. Campo, A. D. Valentine, C. J. Walsh, J. A. Lewis, *Adv. Mater.* **2015**, *27*, 2440.
[3] L. Cai, L. Song, P. Luan, Q. Zhang, N. Zhang, Q. Gao, D. Zhao, X. Zhang, M. Tu, F. Yang, *Sci. Rep.* **2013**, *3*, 3048.
[4] T. Yamada, Y. Hayamizu, Y. Yamamoto, Y. Yomogida, A. Izadi-Najafabadi, D. N. Futaba, K. Hata, *Nat. Nanotechnol.* **2011**, *6*, 296.
[5] S. Ryu, P. Lee, J. B. Chou, R. Xu, R. Zhao, A. J. Hart, S.-G. Kim, *ACS Nano* **2015**, *9*, 5929.
[6] S. J. Preece, L. P. Kenney, M. J. Major, T. Dias, E. Lay, B. T. Fernandes, *J. Neuroeng. Rehabil.* **2011**, *8*, 32.
[7] J. B. Gafford, R. J. Wood, C. J. Walsh, *IEEE Sens. J.* **2016**, *16*, 69.
[8] M. Amjadi, A. Pichitpajongkit, S. Lee, S. Ryu, I. Park, *ACS Nano* **2014**, *8*, 5154.
[9] C. Yan, J. Wang, W. Kang, M. Cui, X. Wang, C. Y. Foo, K. J. Chee, P. S. Lee, *Adv. Mater.* **2014**, *26*, 2022.
[10] M. D. Bartlett, E. J. Markvicka, C. Majidi, *Adv. Funct. Mater.* **2016**, *26*, 8496.
[11] J. C. Yeo, H. K. Yap, W. Xi, Z. Wang, C.-H. Yeow, C. T. Lim, *Adv. Mater. Technol.*, **2016**, *1*, 1600018.
[12] O. Atalay, W. R. Kennon, E. Demirok, *IEEE Sens. J.* **2015**, *15*, 110.
[13] Y. Wang, L. Wang, T. Yang, X. Li, X. Zang, M. Zhu, K. Wang, D. Wu, H. Zhu, *Adv. Funct. Mater.* **2014**, *24*, 4666.
[14] R. Paradiso, G. Loriga, N. Taccini, *IEEE Trans. Inform. Technol. Biomed.* **2005**, *9*, 337.
[15] D. Rus, M. T. Tolley, *Nature* **2015**, *521*, 467.
[16] R. Slyper, I. Poupyrev, J. Hodgins, in *Proc. of the Fifth Int. Conf. on Tangible, Embedded, and Embodied Interaction*, ACM, New York **2011**.
[17] N. Lu, C. Lu, S. Yang, J. Rogers, *Adv. Funct. Mater.* **2012**, *22*, 4044.
[18] N. Bowden, S. Brittain, A. G. Evans, J. W. Hutchinson, G. M. Whitesides, *Nature* **1998**, *393*, 146.
[19] Y. Sun, V. Kumar, I. Adesida, J. A. Rogers, *Adv. Mater.* **2006**, *18*, 2857.
[20] D. S. Gray, J. Tien, C. S. Chen, *Adv. Mater.* **2004**, *16*, 393.

[21] F. Xu, W. Lu, Y. Zhu, *ACS Nano* **2010**, *5*, 672.
[22] S. Chung, J. Lee, H. Song, S. Kim, J. Jeong, Y. Hong, *Appl. Phys. Lett.* **2011**, *98*, 153110.
[23] Y. Su, X. Ping, K. J. Yu, J. W. Lee, J. A. Fan, B. Wang, M. Li, R. Li, D. V. Harburg, Y. Huang, *Adv. Mater.* **2017**, *29*, 1604989.
[24] D. H. Kim, J. Xiao, J. Song, Y. Huang, J. A. Rogers, *Adv. Mater.* **2010**, *22*, 2108.
[25] C. F. Guo, T. Sun, Q. Liu, Z. Suo, Z. Ren, *Nat. Commun.* **2014**, *5*, 3121.
[26] T. Q. Trung, N. E. Lee, *Adv. Mater.* **2016**, *28*, 4338
[27] Y. Zhu, F. Xu, *Adv. Mater.* **2012**, *24*, 1073.
[28] Y. Zhu, J. Moran-Mirabal, *Adv. Electron. Mater.* **2016**, *2*, 1500345
[29] S. J. Park, J. Kim, M. Chu, M. Khine, *Adv. Mater. Technol.* **2016**, *1*, 1600053.
[30] J. Lee, S. Chung, H. Song, S. Kim, Y. Hong, *J. Phys. D: Appl. Phys.* **2013**, *46*, 105305.
[31] C. Yu, H. Jiang, *Thin Solid Films* **2010**, *519*, 818.
[32] D. Maji, D. Das, J. Wala, S. Das, *Sci. Rep.* **2015**, *5*, 17776.
[33] J. Tang, H. Guo, M. Zhao, J. Yang, D. Tsoukalas, B. Zhang, J. Liu, C. Xue, W. Zhang, *Sci. Rep.* **2015**, *5*, 16527.
[34] A. Revzin, R. J. Russell, V. K. Yadavalli, W.-G. Koh, C. Deister, D. D. Hile, M. B. Mellott, M. V. Pishko, *Langmuir* **2001**, *17*, 5440.
[35] J. Lee, S. Kim, J. Lee, D. Yang, B. C. Park, S. Ryu, I. Park, *Nanoscale* **2014**, *6*, 11932.
[36] T. Adrega, S. Lacour, *J. Micromech. Microeng.* **2010**, *20*, 055025.
[37] J. Jeong, S. Kim, J. Cho, D. Kim, Y. Hong, *Jpn. J. Appl. Phys.* **2010**, *49*, 05EB09.
[38] M. Amjadi, K. U. Kyung, I. Park, M. Sitti, *Adv. Funct. Mater.* **2016**, *26*, 1678.
[39] M. Amjadi, M. Turan, C. P. Clementson, M. Sitti, *ACS Appl. Mater. Interfaces* **2016**, *8*, 5618.
[40] J. B. Gafford, R. J. Wood, C. J. Walsh, *2017 IEEE International Conference on Robotics and Automation*, ICRA, Singapore, May **2017**.
[41] H. L. Filiatrault, R. S. Carmichael, R. A. Boutette, T. B. Carmichael, *ACS Appl. Mater. Interfaces* **2015**, *7*, 20745.
[42] P. Mandlik, S. P. Lacour, J. W. Li, S. Y. Chou, S. Wagner, *IEEE Electron Device Lett.* **2006**, *27*, 650.
[43] A. P. Robinson, I. Minev, I. M. Graz, S. P. Lacour, *Langmuir* **2011**, *27*, 4279.
[44] S. C. Mannsfeld, B. C. Tee, R. M. Stoltenberg, C. V. H. Chen, S. Barman, B. V. Muir, A. N. Sokolov, C. Reese, Z. Bao, *Nat. Mater.* **2010**, *9*, 859.
[45] Y. Ding, I. Galiana, A. Asbeck, S. De Rossi, J. Bae, T. Santos, V. Araujo, S. Lee, K. Holt, C. Walsh, *IEEE Trans. Neural Syst. Rehabil. Eng.* **2016**, *1*, 13.
[46] P. Polygerinos, Z. Wang, K. C. Galloway, R. J. Wood, C. J. Walsh, *Rob. Auton. Syst.* **2015**, *73*, 135.
[47] B. Mosadegh, P. Polygerinos, C. Keplinger, S. Wennstedt, R. F. Shepherd, U. Gupta, J. Shim, K. Bertoldi, C. J. Walsh, G. M. Whitesides, *Adv. Funct. Mater.* **2014**, *24*, 2163.
[48] F. A. Panizzolo, I. Galiana, A. T. Asbeck, C. Siviy, K. Schmidt, K. G. Holt, C. J. Walsh, *J. Neuroeng. Rehabil.* **2016**, *13*, 43.
[49] J. Shintake, S. Rosset, B. Schubert, S. Mintchev, D. Floreano, H. R. Shea, *Electroactive Polymer Actuators and Devices*, Vol. *9430*, SPIE, Bellingham, USA **2015**.
[50] S. Li, H. Zhao, R. F. Shepherd, *MRS Bull.* **2017**, *42*, 138.
[51] H. Zhao, K. O'Brien, S. Li, R. F. Shepherd, *Sci. Rob.* **2016**, *1*, eaai7529.

